



HAL
open science

Dark Current Blooming in Pinned Photodiode CMOS Image Sensors

Jean-Marc Belloir, Jean-Baptiste Lincelles, Alice Pelamatti, Clementine Durnez, Vincent Goiffon, Cédric Virmontois, Philippe Paillet, Pierre Magnan, Olivier Gilard

► **To cite this version:**

Jean-Marc Belloir, Jean-Baptiste Lincelles, Alice Pelamatti, Clementine Durnez, Vincent Goiffon, et al.. Dark Current Blooming in Pinned Photodiode CMOS Image Sensors. IEEE Transactions on Electron Devices, 2017, vol. 64 (n° 3), pp. 11161-1166. 10.1109/TED.2017.2654515 . hal-01503707

HAL Id: hal-01503707

<https://hal.science/hal-01503707>

Submitted on 7 Apr 2017

HAL is a multi-disciplinary open access archive for the deposit and dissemination of scientific research documents, whether they are published or not. The documents may come from teaching and research institutions in France or abroad, or from public or private research centers.

L'archive ouverte pluridisciplinaire **HAL**, est destinée au dépôt et à la diffusion de documents scientifiques de niveau recherche, publiés ou non, émanant des établissements d'enseignement et de recherche français ou étrangers, des laboratoires publics ou privés.



Open Archive TOULOUSE Archive Ouverte (OATAO)

OATAO is an open access repository that collects the work of Toulouse researchers and makes it freely available over the web where possible.

This is an author-deposited version published in: <http://oatao.univ-toulouse.fr/>
Eprints ID: 17373

To cite this version: Belloir, Jean-Marc and Lincelles, Jean-Baptiste and Pelamatti, Alice and Durnez, Clementine and Goiffon, Vincent and Virmontois, Cédric and Paillet, Philippe and Magnan, Pierre and Gilard, Olivier *Dark Current Blooming in Pinned Photodiode CMOS Image Sensors*. (2017) IEEE Transactions on Electron Devices, vol. PP (n° 99). pp. 1-6. ISSN 0018-9383

Official URL: <http://dx.doi.org/10.1109/TED.2017.2654515>

Any correspondence concerning this service should be sent to the repository administrator: staff-oatao@listes-diff.inp-toulouse.fr

Dark Current Blooming in Pinned Photodiode CMOS Image Sensors

Jean-Marc Belloir, *Student Member, IEEE*, Jean-Baptiste Lincelles, Alice Pelamatti, Clémentine Durnez, *Student Member, IEEE*, Vincent Goiffon, *Member, IEEE*, Cédric Virmondois, *Member, IEEE*, Philippe Paillet, *Senior Member, IEEE*, Pierre Magnan, *Member, IEEE*, and Olivier Gilard, *Member, IEEE*

Abstract—This paper demonstrates the existence of dark current blooming in pinned photodiode (PPD) CMOS image sensors (CISs) with the support of both experimental measurements and TCAD simulations. It is usually assumed that blooming can appear only under illumination, when the charge collected by a pixel exceeds the full well capacity (FWC) (i.e., when the photodiode becomes forward biased). In this paper, it is shown that blooming can also appear in the dark by dark current leakage from hot pixels in reverse bias (i.e., below the FWC). The dark current blooming is observed to propagate up to nine pixels away in the experimental images and can impact hundreds of pixels around each hot pixel. Hence, it can be a major image quality issue for the state-of-the-art PPD CISs used in dark current limited applications, such as low-light optical imaging and should be considered in the dark current subtraction process. This paper also demonstrates that one of the key parameter for dark current optimization, the transfer gate bias during integration, has to be carefully chosen depending on the application because the optimum bias for dark current reduction leads to the largest dark current blooming effects.

Index Terms—Active pixel sensor, blooming, dark current, CMOS image sensor (CIS), diffusion current, full well capacity (FWC), pinned photodiode (PPD), p-n junction, reverse bias, thermionic emission.

I. INTRODUCTION

CMOS image sensors (CISs) have become the main optical imaging technology for a wide variety of consumer and high-end scientific applications. In particular, the state-of-the-art pinned photodiode (PPD) [1]–[3] CIS now provides pixels with extremely low intrinsic dark current (on the order of the e-/s at room temperature for the devices tested here) thanks to elaborated structural and operational improvements [4]–[7].

Manuscript received August 16, 2016; revised December 22, 2016; accepted January 11, 2017. The review of this paper was arranged by Editor A. Bermak.

J.-M. Belloir, J.-B. Lincelles, C. Durnez, V. Goiffon, and P. Magnan are with ISAE, Image Sensor Research Team, Université de Toulouse, F-31055 Toulouse, France (e-mail: jean-marc.belloir@isae.fr; vincent.goiffon@isae.fr; pierre.magnan@isae.fr).

A. Pelamatti is with Airbus Defence and Space, F-31402 Toulouse, France (e-mail: alice.pelamatti@airbus.com).

P. Paillet is with CEA, DAM, DIF, F-91297 Arpajon, France (e-mail: philippe.paillet@cea.fr; melanie.raine@cea.fr).

C. Virmondois and O. Gilard are with CNES, F-31400 Toulouse, France (e-mail: cedric.virmondois@cnes.fr; olivier.gilard@cnes.fr).

Color versions of one or more of the figures in this paper are available online at <http://ieeexplore.ieee.org>.

Digital Object Identifier 10.1109/TED.2017.2654515

These enhancements allow them to be considered in an increasing number of low-light imaging applications. In the past years, significant efforts have been made to better understand the electrical properties and functioning of the PPD, especially regarding the pinning voltage, the PPD capacitance, the full well capacity (FWC), the transfer gate (TG) functioning, and the charge transfer efficiency [8]–[16].

Nowadays, the low-light performance of the state-of-the-art PPD CIS remains mainly limited by “hot” pixels, which have a higher dark current than the mean dark current of the pixel array (and thus, a lower dynamic range and sensitivity). For most of them, the higher dark current is due to the presence of one or several Shockley–Read–Hall recombination-generation (SRH R-G) centers [17] in the depletion region of the photodiode, which thermally generate electron–hole pairs when $pn - n_i^2 < 0$ (where p and n are the hole and electron concentrations and n_i is the intrinsic free carrier concentration). This condition is verified only when the p-n junction of the PPD is reverse biased, i.e., when the charge stored in the PPD is lower than the equilibrium FWC (EFCWC), which is charge stored in the PPD at equilibrium (i.e., for zero bias) [12]. The highest reverse bias of the PPD is called the pinning voltage [12] and is reached when the PPD is completely empty.

On the other hand, blooming effects in CIS are usually expected to appear only in forward bias, i.e., when the charge stored in the PPD is higher than the EFCWC [12]. Indeed, it is only in forward bias that the net current through a p-n junction is positive, i.e., that more electrons flow from the n side to the p side than from the p side to the n side [18]. In that case, there are more electrons flowing from the PPD to the epitaxy than from the epitaxy to the PPD, which means that electrons are leaking from the PPD to the epitaxy, and eventually, they are collected by the surrounding pixels. The PPD can become forward biased (collected charge higher than the EFCWC) under illumination, but also with effects, such as electroluminescence or impact ionization by hot carrier injection [19], which act, respectively, as external sources of photons and excess minority carriers. Similar to light, these effects can overflow the impacted pixels and produce light-like blooming in the dark. However, in the dark and without these effects, the charge stored in the PPD cannot exceed the EFCWC (and the photodiode cannot become forward biased), because the generation rate of SRH R-G centers cancels at equilibrium ($pn - n_i^2 = 0$) [17]. For these reasons, it is usually assumed

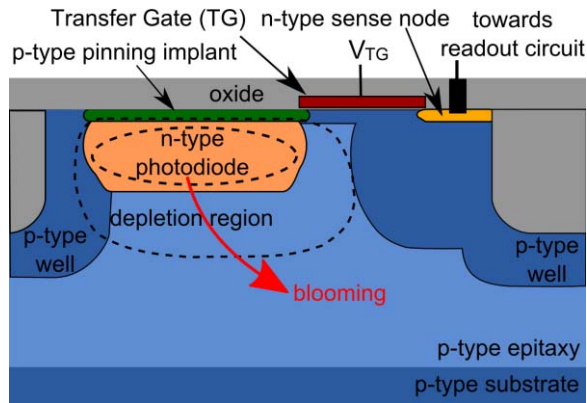


Fig. 1. Schematic cross section of a 4T-PPD pixel. The readout circuit contains three transistors (not represented here) used to sample the output voltage of the floating diffusion.

that hot pixels cannot produce dark current blooming (i.e., that the dark current generated by hot pixels cannot leak toward neighboring pixels).

In this paper, it is shown that dark current blooming is possible in PPD CIS contrary to what is usually believed. Indeed, it is shown that blooming can exist for small reverse biases, allowing the dark current generated in hot pixels to leak toward surrounding pixels. The dark current blooming is observed to propagate up to nine pixels away from hot pixels, potentially impacting hundreds of pixels around each hot pixel. Therefore, the dark current blooming can have major effects on low-light images and should be considered in the dark current subtraction process.

II. DEVICES UNDER TEST

Two custom four-transistor PPD (4T-PPD) CIS is tested in this paper. These devices are fabricated in a commercially available $0.18\text{-}\mu\text{m}$ technology dedicated to imaging and are made of 256×256 pixel arrays with different pixel pitches (4.5 and $7\ \mu\text{m}$). Fig. 1 shows the schematic cross section of a typical 4T-PPD pixel. The PPD can be seen as a spherical p-n junction formed by an n-type photodiode encapsulated in a grounded (biased at $0\ \text{V}$) p-type silicon. When light impinges on the pixel, the photo-generated electrons are collected by the p-n junction and stored in the n-type photodiode. At the end of the exposure time, the electrons are transferred to the floating diffusion by applying a positive TG bias ($V_{\text{TG}} = 3.3\ \text{V}$ here), which empties the photodiode. The floating diffusion allows converting the signal from the charge domain to the voltage domain and the output signal is a voltage proportional to the collected charge. The PPD electrostatic potential (V_{PPD}) corresponds to the reverse bias of the p-n junction formed by the photodiode and the surrounding p-type silicon (which is grounded): it is positive in reverse bias (when the collected charge is lower than the EFWC) and negative in forward bias.

III. EXPERIMENTAL RESULTS

A. Long Integration Time Images

First of all, Fig. 2 shows frame crops acquired with both CIS in the dark and with long integration (exposure) times. Blooming effects are clearly visible around all the hot pixels

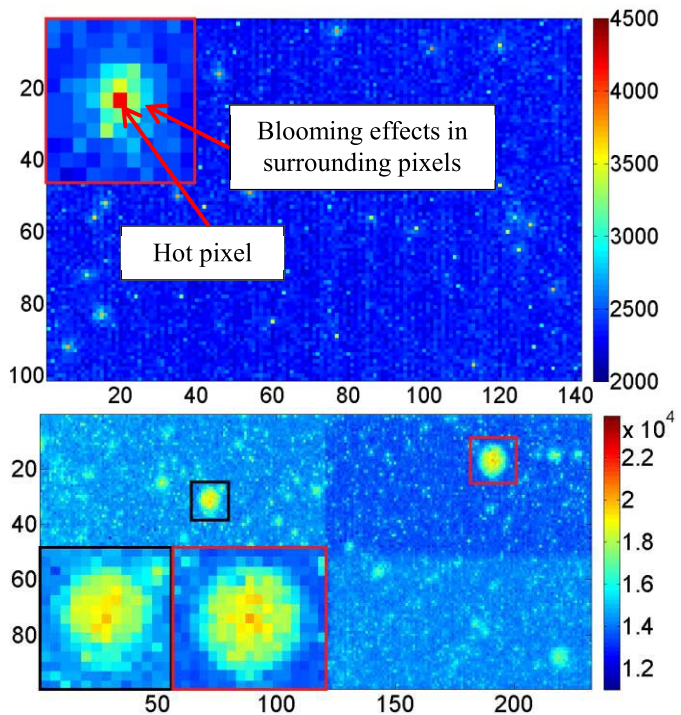


Fig. 2. Dark frames (in electrons) in (a) $4.5\text{-}\mu\text{m}$ pixel pitch CIS and (b) $7\text{-}\mu\text{m}$ pixel pitch CIS with exposure times of, respectively, 13 and 25 s and at temperatures of, respectively, $50\ ^\circ\text{C}$ and $60\ ^\circ\text{C}$.

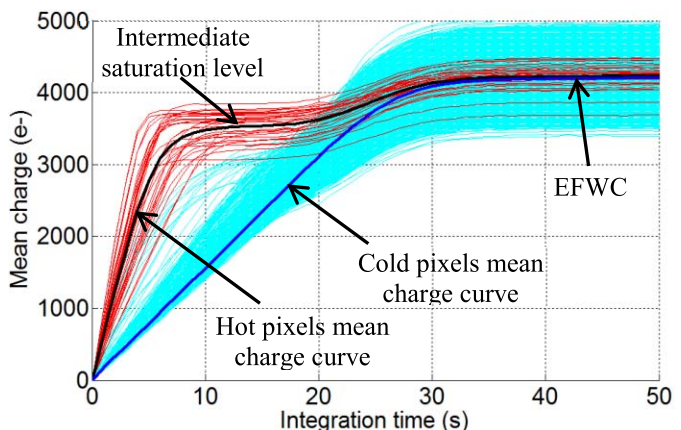


Fig. 3. Integrated charge as a function of integration time in the dark for all the pixels of the $4.5\text{-}\mu\text{m}$ pixel pitch CIS at $50\ ^\circ\text{C}$.

of both CIS, and the magnified areas show that many pixels can be impacted around the hottest pixels. Hence, blooming effects seem possible in the dark around all regular SRH R-G hot pixels in a 4T-PPD CIS.

Fig. 3 shows the integrated charge of each pixel of the $4.5\text{-}\mu\text{m}$ pixel pitch CIS depending on the integration time in the dark. The pixels, which have a dark current (measured before saturation) higher than twice the mean dark current of the CIS, are considered as hot pixels, as opposed to the other pixels which will be called “cold” pixels. For very long integration times ($>30\ \text{s}$), both hot and cold pixels reach a similar final saturation level, which is the EFWC. Indeed, after a very long time spent in the dark, all the photodiodes have returned to equilibrium by integrating their dark current.

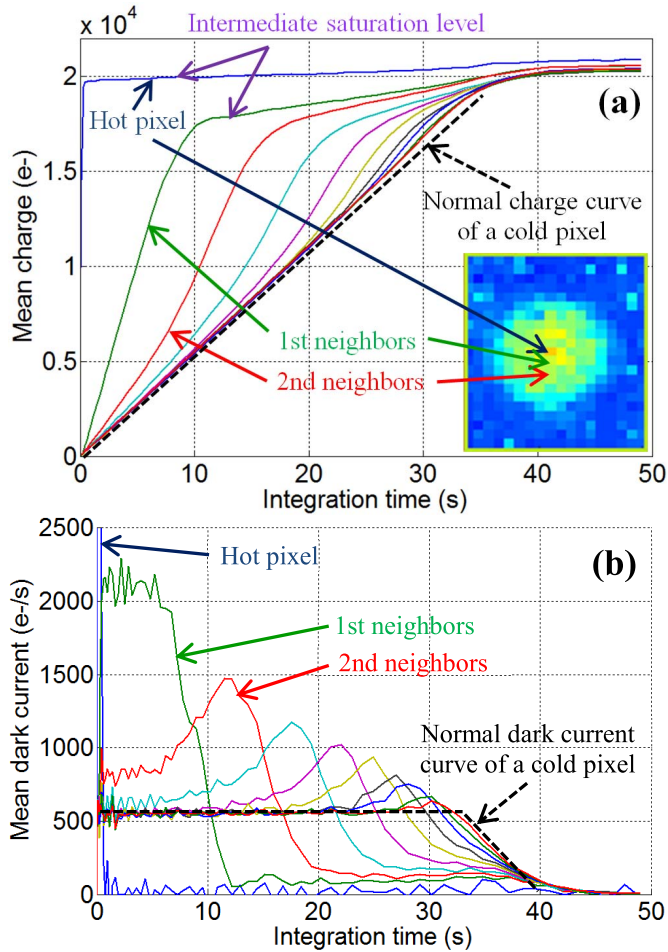


Fig. 4. (a) Charge and (b) dark current of a hot pixel and its surrounding pixels as a function of integration time in the dark at $T = 60^\circ\text{C}$ in the $7\text{-}\mu\text{m}$ pixel pitch CIS.

For integration times between 10 and 20 s, an intermediate saturation level lower than the EFWC is observed for hot pixels and persists until the cold pixels reach a similar charge level. At the intermediate level, the PPD of a hot pixel is reverse biased (which corresponds to a positive PPD potential), because the charge is lower than the EFWC. Thus, the PPD has a positive dark current I_{dark} , which is mainly due to the generation current of SRH R-G centers for a hot pixel, and which can be simply expressed as [18]

$$I_{\text{dark}} = I_{0,\text{dark}} \left[1 - \exp\left(-\frac{qV_{\text{PPD}}}{2kT}\right) \right] \text{ for } V_{\text{ppd}} > 0. \quad (1)$$

In (1), V_{PPD} is the PPD potential and $I_{0,\text{dark}}$ is the maximum dark current of the pixel reached at high reverse biases ($qV_{\text{PPD}} \gg 2kT$). The idea that the integrated charge in the hot pixels is constant in the intermediate level suggests that the dark current (positive under reverse bias) is compensated by another current leaking out of the PPD. This hypothesis is supported by the idea that the blooming effects observed on the dark frames (Fig. 2) appear for integration times between 10 and 20 s, which corresponds to the situation where hot pixels are at the intermediate saturation level.

Fig. 4 shows the integrated charge and the dark current as a function of integration time for a $7\text{-}\mu\text{m}$ pixel pitch CIS hot

pixel, as well as the mean charge and the mean dark current of its surrounding pixels depending on their distance from the hot pixel. The first neighbors correspond to pixels adjacent to the hot pixel, the second neighbors correspond to pixels adjacent to the first neighbors, and so on. The normal dark current of the CIS (mean dark current of the cold pixels) is 550 e-/s at $T = 60^\circ\text{C}$, whereas it is about 50000 e-/s for the hot pixel studied here. As soon as the hot pixel reaches the intermediate level [about 20 kilo electrons (ke-) after 0.4 s, Fig. 4(a)], a large dark current rise is visible in the first neighbors [from 550 to more than 2000 e-/s , Fig. 4(b)] and their charge increases more rapidly than the normal charge curve of cold pixels [Fig. 4(a)]. A slight dark current rise is also visible in the second and third neighbors, which suggests that the dark current of the hot pixel is leaking in the epitaxy and can diffuse several pixels away in the epitaxy before being collected by surrounding pixels. After about 10 s, the first neighbors also reach the intermediate level [18 ke-, Fig. 4(a)] and a dark current rise is observed in the second neighbor. Successive dark current augmentations are visible in the surrounding pixels at increasing distances from the hot pixel [Fig. 4(b)], which shows that the dark current leaks from pixels that reach the intermediate level and propagates toward further pixels by diffusing in the epitaxy. The dark current blooming is observed up to nine pixels away from the hot pixel [Fig. 4(b)], at which point all the cold pixels of the CIS reach the intermediate saturation level [at about 30 s, Fig. 4(a)]. After that, the dark current blooming stops and both hot and cold pixels reach the EFWC [$\sim 21\text{ ke-}$ after about 40 s, Fig. 4(a)]. In conclusion, the analysis of the long integration time images in the two PPD CIS suggests that blooming is possible in reverse bias, and that the dark current blooming from hot pixels is responsible for the observed blooming effects on the images.

B. Effect of Temperature

Fig. 5 shows the average integrated charge of all the hot pixels of the $4.5\text{-}\mu\text{m}$ pixel pitch CIS as a function of integration time in the dark and at different temperatures. The EFWC (final saturation level) increases with temperature, which is expected due to the increase of the pinning voltage [12]. On the contrary, the intermediate saturation level reduces with temperature, which means that the PPD potential at this level increases with temperature (i.e., higher reverse bias). In this level, it has been assumed that the dark current of the PPD [generation current given by (1)] is balanced by a leakage current toward the surrounding pixels. This leakage current can be explained by an electron diffusion current within the epitaxy. Indeed, the diffusion current I_{diff} of the p-n junction formed by the PPD and the epitaxy can be expressed as [18]

$$I_{\text{diff}} = I_{0,\text{diff}} \exp\left(-\frac{qV_{\text{PPD}}}{kT}\right). \quad (2)$$

In (2), $I_{0,\text{diff}}$ is the diffusion current at equilibrium. This equation shows that the diffusion current is nonnegligible at small reverse bias (it is permitted by thermionic emission over the p-n junction potential barrier [14]). Once electrons have been emitted from the hot pixel PPD to the epitaxy,

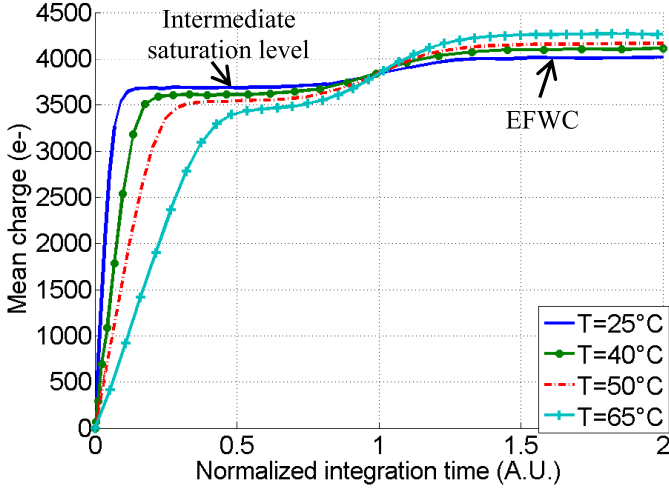


Fig. 5. Average charge curve of all the hot pixels of the 4.5- μm pixel pitch CIS in the dark at different temperatures. For each curve, the integration time is normalized with respect to the transition between the intermediate saturation level and the EFCW for clarity purposes.

they can diffuse toward surrounding pixels. In the low doped p-type epitaxy (typically 10^{15} cm^{-3}), the electron diffusion length [18] (typically $100 \mu\text{m}$ for 10^{15} cm^{-3}) is much larger than the distance between two PPD (which is roughly equal to the pixel pitch). Hence, the diffusion current can be approximated by the “short diode” model [18], which corresponds to a diffusion limited thermionic emission [20]. In that case, the recombination within the epitaxy is negligible and all the electrons emitted by the hot pixel are collected by the surrounding pixels (the diffusion current of the hot pixel photodiode equals the sum of the drift currents of the surrounding pixels photodiodes). Additionally, the amount of electrons emitted by the surrounding pixels can be considered negligible, because their charge is much lower than the intermediate saturation level. Hence, their reverse bias is higher and their diffusion current is negligible from (2). Thus, there are only two electron currents in the hot pixel PPD: the generation (dark) current filling the PPD and the diffusion limited thermionic emission emptying the PPD. These two currents compensate for a given PPD potential V_{PPDeq} obtained by equating (1) and (2)

$$V_{\text{PPDeq}} = \frac{2kT}{q} \ln \left(\frac{1}{2} \sqrt{\frac{4I_{0,\text{diff}} + I_{0,\text{dark}}}{I_{0,\text{dark}}}} + \frac{1}{2} \right). \quad (3)$$

The PPD potential at the intermediate saturation level V_{PPDeq} increases with temperature, because $I_{0,\text{diff}}$ rises more rapidly with temperature than $I_{0,\text{dark}}$. Indeed, the diffusion current (which is proportional to n_i^2) varies more rapidly than the generation current (which is proportional to n_i), which explains why the intermediate saturation level decreases with temperature. Additionally, it can be seen from (3) that the PPD potential is lower if $I_{0,\text{dark}}$ is higher, which explains why the intermediate saturation level is higher for the hot pixel than for cold pixels, as shown in Fig. 4. Indeed, for hot pixels, the generation current is higher and requires a larger diffusion current (thus a lower reverse bias) to be compensated.

TABLE I
EXPERIMENTAL VARIATION OF THE INTERMEDIATE SATURATION LEVEL AND THE EFCW WITH TEMPERATURE

T (°C)	Intermediate saturation level (e-)	EFCW (e-)	Reverse bias at the intermediate level V_{PPDeq} (mV)
0	3,570 \nearrow	3,810 \nearrow	30 =
10	3,640 \nearrow	3,900 \nearrow	33 =
25	3,680 \nearrow	4,020 \nearrow	42 =
40	3,610 \searrow	4,100 \nearrow	61 \nearrow
50	3,550 \searrow	4,170 \nearrow	78 \nearrow
65	3,470 \searrow	4,270 \nearrow	100 \nearrow

Table I presents the experimental values for the intermediate saturation level and the EFCW extracted from Fig. 5 but also for lower temperatures. Between 25 °C and 65 °C, the intermediate saturation level decreases with temperature as explained earlier. On the other hand, below 25 °C, the intermediate saturation level increases with temperature (i.e., follows the variation of the EFCW). This can be explained by the idea that the reverse bias at which the two currents compensate V_{PPDeq} remains similar at low temperatures. For each temperature, V_{PPDeq} can be estimated from the intermediate saturation level and the EFCW. Indeed, if the PPD capacitance is assumed not to change with PPD potential, then the PPD potential V_{PPD} and the collected charge $Q(V_{\text{PPD}})$ are linked with the EFCW and the pinning voltage V_{pin} by the equation

$$Q(V_{\text{PPD}}) \approx \text{EFCW} \left(1 - \frac{V_{\text{PPD}}}{V_{\text{pin}}} \right). \quad (4)$$

Therefore, if $Q(V_{\text{PPD}})$ is the intermediate saturation level, V_{PPD} corresponds to V_{PPDeq} . For the 4.5 μm -pixel pitch CIS, V_{pin} is about 0.5 V; the estimated values for V_{PPDeq} are reported in Table I. Below 25 °C, V_{PPDeq} remains low (about 30 mV) and does not vary with temperature, which explains why the intermediate saturation level follows the variation of the EFCW (increases with temperature). In conclusion, the analysis of the effect of temperature supports the idea that the blooming effects observed happen in reverse bias conditions and that they correspond to dark current blooming.

IV. TCAD SIMULATIONS

A 2-D TCAD structure comprising three 7- μm pixel pitch 4T-PPD pixels similar to the pixel represented in Fig. 1 was designed to validate the existence of the dark current blooming under simulation. The doping concentration of the elementary pixel in this structure is represented in Fig. 6. First of all, a quasi-stationary simulation is performed with the middle pixel in the integration mode (TG OFF, $V_{\text{TG}} = -0.2 \text{ V}$) and the two surrounding pixels in the reset mode (TG ON, $V_{\text{TG}} = 3.3 \text{ V}$). In this state, the middle pixel (which represents a hot pixel) should reach the EFCW while the surrounding pixels (which represent cold pixels) are still empty. Fig. 7(a) shows that a generation current still exists in the PPD of the middle pixel, in agreement with the slightly positive PPD potential (about 30 mV here). In Fig. 7(b), it can be seen

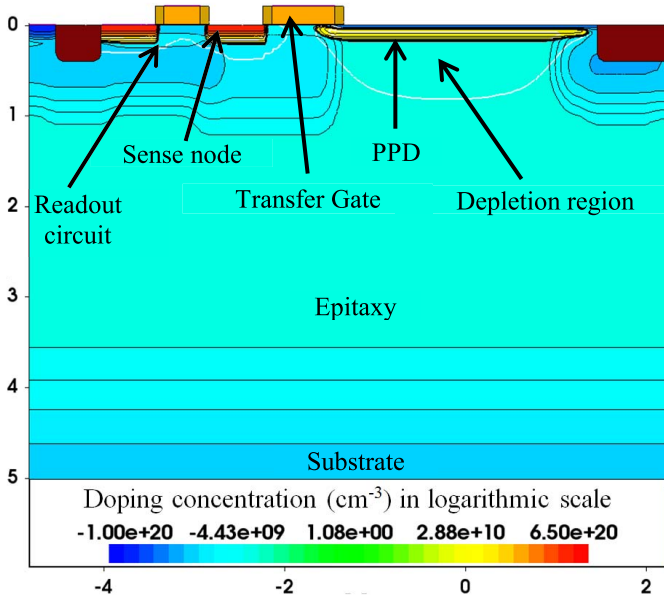


Fig. 6. 2-D TCAD doping structure of the 7- μm pixel pitch 4T-PPD pixel. This structure is repeated three times to form the complete simulated structure.

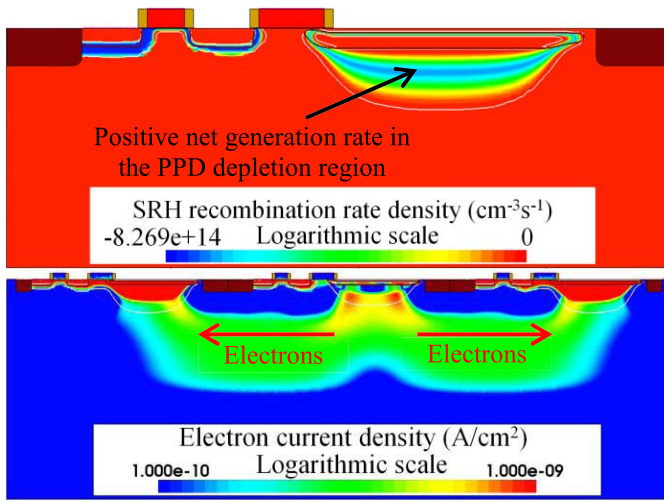


Fig. 7. Results of the quasi-stationary TCAD simulation in the dark ($T = 25\text{ }^\circ\text{C}$) with the middle pixel in the integration mode and the surrounding pixels in the reset mode. (a) SRH recombination rate in the middle pixel. (b) Electron current density in the whole structure.

that an electron current is diffusing from the middle pixel toward the surrounding pixels through the epitaxy. The total diffusion current is equal to the generation current in the middle pixel in Fig. 7(a), hence, the dark current of the hot pixel is leaking to the surrounding pixels. The PPD potential of the hot pixel is slightly positive (reverse bias) and the integrated charge in the PPD ($8900\text{ e-}/\mu\text{m}$ in the direction perpendicular to Figs. 6 and 7) is also lower than the EFWC ($9500\text{ e- per } \mu\text{m}$); this confirms that the dark current blooming occurs in reverse bias at an intermediate saturation level. This simulation was performed at different temperatures in order to study the evolution of the intermediate saturation level and of the EFWC with temperature. As reported in Table II, the EFWC always increases with temperature as

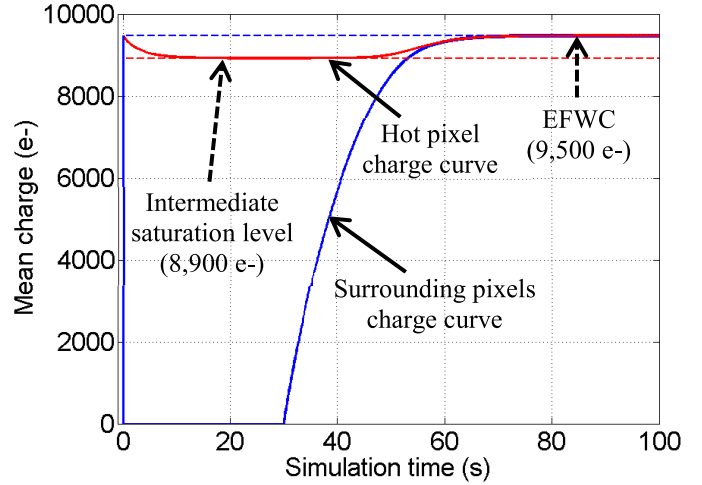


Fig. 8. Charge in the middle and surrounding pixels during the transient simulation in the dark ($T = 300\text{ K}$).

experimentally observed (Table I). On the other hand, the intermediate saturation level increases with temperature at low temperature (like experimental results) and remains similar at higher temperatures, showing that it does not follow the variation of the EFWC at high temperature. The PPD potential (reverse bias at the intermediate saturation level) increases with temperature as observed experimentally.

Fig. 8 shows the integrated charge of the middle pixel (hot pixel) and the surrounding pixels during a transient simulation. The simulation starts from a pseudoequilibrium state with all the pixels in integration mode, i.e., at EFWC (9500 e-). At 0 s, the surrounding pixels are put in reset mode and the middle pixel is kept in integration mode. Because of the dark current blooming, the charge of the middle pixel reduces from the EFWC (9500 e- and $V_{\text{PPD}} = 0\text{ V}$) to the intermediate level (8900 e- and $V_{\text{PPD}} > 0\text{ V}$), which corresponds to the charge of the middle pixel in the quasi-stationary simulation of Fig. 7. At 30 s, the surrounding pixels are put back in integration mode. The dark current blooming persists (the middle pixel stays at the intermediate saturation level) until the surrounding pixels also reach this level ($\sim 50\text{ s}$); then, all the pixels go back to the EFWC. In conclusion, the TCAD simulations agree with the experimental results and show that the blooming effects can be explained by the dark current blooming at small reverse bias.

V. DARK CURRENT BLOOMING COUNTERMEASURE

The effect of the TG bias (V_{TG}) during integration on the dark current blooming has been investigated (Fig. 9). A slight negative bias (-0.2 V in this paper) is usually chosen for low-light imaging because it ensures a very low mean dark current of the CIS. Indeed, the oxide interface under the TG is mainly accumulated with holes in that case, which neutralize the interface generation centers [15]. However, the potential barrier under the TG is higher than the potential barrier between the PPD and the epitaxy, because the substrate is grounded (0 V). Therefore, the dark current of the PPD is rather emitted toward the epitaxy than under the TG by

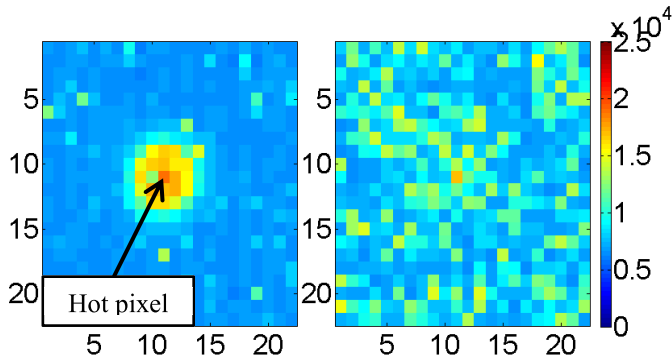


Fig. 9. Dark frames of an identical region of the 7- μm pixel pitch CIS, in identical experimental conditions except the TG bias during integration: -0.2 V on the left and $+0.2\text{ V}$ on the right.

TABLE II

SIMULATED VARIATION OF THE INTERMEDIATE SATURATION LEVEL AND THE EFWC WITH TEMPERATURE

T ($^{\circ}\text{C}$)	Intermediate saturation level (e-)	EFWC (e-)	Reverse bias at the intermediate level (mV)
10	8,680 ↗	8,920 ↗	14 =
25	8,900 ↗	9,410 ↗	31 ↗
40	9,010 ↗	9,820 ↗	49 ↗
50	9,030 =	10,030 ↗	60 ↗
65	9,040 =	10,270 ↗	74 ↗
80	9,030 =	10,450 ↗	86 ↗

thermionic emission, which leads to the dark current blooming (Fig. 9). If the TG is biased positively ($+0.2\text{ V}$ in Fig. 9), which is a common light induced blooming countermeasure, the potential barrier under the TG becomes lower than toward the epitaxy and the dark current will rather diffuse under the TG (and will be collected by the floating diffusion) than toward the epitaxy. In that case, it can be seen in Fig. 9 that the dark current blooming is suppressed. However, the mean dark current of the CIS is higher due to the depleted oxide interface under the TG.

VI. CONCLUSION

The existence of the dark current blooming in 4T-PPD CIS has been demonstrated based on both experimental measurements and TCAD simulations. All the results are in agreement with the analytical theory of the p-n junction and suggest that blooming is possible for small reverse bias. Hence, the dark current generated by SRH R-G hot pixels can leak toward surrounding pixels through the epitaxy. This effect, permitted by thermionic emission over the p-n junction potential barrier followed by the diffusion of electrons in the epitaxy, can produce blooming effects in hundreds of pixels around each hot pixel. Hence, it seems critical to take the dark current blooming into account when performing the dark signal

subtraction in long integration time images, e.g., for low-light imaging. Increasing the TG bias during integration suppresses the dark current blooming but strongly increases the overall dark current of the CIS, hence this setting should be carefully chosen depending on the application.

REFERENCES

- [1] N. Teranishi, A. Kohono, Y. Ishihara, E. Oda, and K. Arai, "No image lag photodiode structure in the interline CCD image sensor," in *IEDM Tech. Dig.*, vol. 28. Dec. 1982, pp. 324–327.
- [2] B. C. Burksey *et al.*, "The pinned photodiode for an interline-transfer CCD image sensor," in *IEDM Tech. Dig.*, vol. 30. Dec. 1984, pp. 28–31.
- [3] E. R. Fossum and D. B. Hondongwa, "A review of the pinned photodiode for CCD and CMOS image sensors," *IEEE J. Electron Devices Soc.*, vol. 2, no. 3, pp. 33–43, May 2014.
- [4] B. Mheen, Y.-J. Song, and A. J. P. Theuwissen, "Negative offset operation of four-transistor CMOS image pixels for increased well capacity and suppressed dark current," *IEEE Electron Device Lett.*, vol. 29, no. 4, pp. 347–349, Apr. 2008.
- [5] T. Watanabe, J.-H. Park, S. Aoyama, K. Isobe, and S. Kawahito, "Effects of negative-bias operation and optical stress on dark current in CMOS image sensors," *IEEE Trans. Electron Devices*, vol. 57, no. 7, pp. 1512–1518, Jul. 2010.
- [6] S.-H. Park *et al.*, "Decrease of dark current by reducing transfer transistor induced partition noise with localized channel implantation," *IEEE Electron Device Lett.*, vol. 31, no. 11, pp. 1278–1280, Nov. 2010.
- [7] N. Teranishi, "Effect and limitation of pinned photodiode," *IEEE Trans. Electron Devices*, vol. 63, no. 1, pp. 10–15, Jan. 2016.
- [8] A. Krymski and K. Feklistov, "Estimates for scaling of pinned photodiodes," in *Proc. IEEE Workshop CCD Adv. Image Sensors*, Jun. 2005, pp. 60–63.
- [9] S. Park and H. Uh, "The effect of size on photodiode pinch-off voltage for small pixel CMOS image sensors," *Microelectron. J.*, vol. 40, no. 1, pp. 137–140, Jan. 2009.
- [10] C. Y.-P. Chao, Y.-C. Chen, K.-Y. Chou, J.-J. Sze, F.-L. Hsueh, and S.-G. Wu, "Extraction and estimation of pinned photodiode capacitance in CMOS image sensors," *IEEE J. Electron Devices Soc.*, vol. 2, no. 4, pp. 59–64, Jul. 2014.
- [11] V. Goiffon *et al.*, "Pixel level characterization of pinned photodiode and transfer gate physical parameters in CMOS image sensors," *IEEE J. Electron Devices Soc.*, vol. 2, no. 4, pp. 65–76, Jul. 2014.
- [12] A. Pelamatti *et al.*, "Temperature dependence and dynamic behavior of full well capacity in pinned photodiode CMOS image sensors," *IEEE Trans. Electron Devices*, vol. 62, no. 4, pp. 1200–1207, Apr. 2015.
- [13] C. Cao, B. Shen, B. Zhang, L. Wu, and J. Wang, "An improved model for the full well capacity in pinned photodiode CMOS image sensors," *IEEE J. Electron Devices Soc.*, vol. 4, no. 3, pp. 306–310, Jul. 2015.
- [14] L. Han, S. Yao, and A. J. P. Theuwissen, "A charge transfer model for CMOS image sensors," *IEEE Trans. Electron Devices*, vol. 1, no. 63, pp. 32–41, Jan. 2016.
- [15] A. Pelamatti *et al.*, "Comparison of pinning voltage estimation methods in pinned photodiode CMOS image sensors," *IEEE J. Electron Devices Soc.*, vol. 4, no. 2, pp. 99–108, Mar. 2016.
- [16] M. Sarkar, B. Büttgen, and A. J. P. Theuwissen, "Temperature effects on feedforward voltage in standard CMOS pinned photodiodes," *IEEE Trans. Electron Devices*, vol. 5, no. 63, pp. 1963–1968, May 2016.
- [17] C.-T. Sah, R. N. Noyce, and W. Shockley, "Carrier generation and recombination in P-N junctions and P-N junction characteristics," *Proc. IRE*, vol. 45, no. 9, pp. 1228–1243, Sep. 1957.
- [18] S. M. Sze, *Semiconductor Devices: Physics and Technology*. Hoboken, NJ, USA: Wiley, 2008.
- [19] S. Maestre, P. Magnan, F. Lavernhe, and F. Corbiere, "Hot carriers effects and electroluminescence in the CMOS photodiode active pixel sensors," *Proc. SPIE*, vol. 5017, pp. 59–67, May 2003.
- [20] P. Biljanovic and T. Suligoj, "Thermionic emission process in carrier transport in PN homojunctions," in *Proc. Electrotechn. Conf. (MELECON)*, May 2000, pp. 248–251.